Fatigue Assessment of Marine Structures

Chapter · January 2011

DOI: 10.13140/RG.2.1.3185.0488

4 authors:

Yordan Garbatov
University of Lisbon
266 PUBLICATIONS **2,126** CITATIONS
SEE PROFILE

Smiljko Rudan
University of Zagreb
36 PUBLICATIONS **164** CITATIONS
SEE PROFILE

Bruno Gaspar
University of Lisbon
23 PUBLICATIONS **140** CITATIONS
SEE PROFILE

Carlos Guedes Soares
University of Lisbon
1,589 PUBLICATIONS **16,204** CITATIONS
SEE PROFILE

Marine Technology and Engineering – Guedes Soares et al. (Eds)
© 2011 Taylor & Francis Group, London, ISBN 978-0-415-69808-5

Fatigue assessment of marine structures

Y. Garbatov
Centre for Marine Technology and Engineering, (CENTEC), Instituto Superior Técnico, Technical University of Lisbon, Portugal

S. Rudan
Faculty of Mechanical Engineering and Naval Architecture, University of Zagreb, Croatia

B. Gaspar & C. Guedes Soares
Centre for Marine Technology and Engineering, (CENTEC), Instituto Superior Técnico, Technical University of Lisbon, Portugal

ABSTRACT: This paper reviews recently developed models for fatigue damage of marine structures accounting for several structural imperfections and different types of loadings. The studied imperfections are generally present in the stress response characteristics and fatigue damage model applied. Besides commonly present uncertainties in fatigue ship structural analysis associated with structural modelling and the random wave induced loading there are also uncertainties arising from imperfection of structural joint that may occur during manufacturing and service life and the interaction between wave induced load and structure. The paper discuses the influence of the imperfections over the hot spot stress distribution and not with the reasons for their appearance. The long-term stress range acting on the elements is defined within a stochastic analysis as a function of wave induced pressure stresses that are combined with the stresses resulting from the vertical wave induced bending moment of the ship hull. Structural analysis is performed by the finite element method utilizing sub-model techniques. This work also deals with the fatigue assessment of marine structures, describing several steps of the calculation accounting for the combination of low- and high-frequency induced loading. Fatigue damage is calculated based on the Palgrem-Miner approach.

1 INSTRUCTION

Fatigue is an important design criterion for welded components and global structures. The fatigue damage may even further reduce the structural resistance with the presence of different kind of imperfections, which can lead to local increasing of the stresses and acceleration of fatigue crack initiation and propagation.

It is therefore of importance to account for different kind imperfections determining the hot spot stress distribution of welded structures due presence.

However, important uncertainties in fatigue damage assessment may arise from human error during the design, construction, exploitation, inspection and maintenance process as far as during the life time of structure. Such uncertainties may be considered in a different manner during the a long-term performance of the structure, but in this paper, only the thickness change misalignment, angular imperfection, rotation of the transverse weld, set of residual deformations that may result due dropped object on deck and a combination of them will be considered in the study performed.

For fatigue life assessments different procedures have been developed based on databases of fatigue behaviour of welded structural components as a result of both tests and theoretical investigations (Fricke and Petershagen, 1992).

The main steps in fatigue analysis are based on direct calculations that involve the description of the wave induced loading (Guedes Soares and Moan, 1991) the stress distribution in the structure (Guedes Soares, et al. 2003), the model of fatigue damage (S-N approach) or fracture mechanics approach (Paris and Erdogan, 1963) and the probabilistic evaluation of the different steps to arrive at a safety index or time dependent reliability as has been developed by Garbatov and Guedes Soares, (1998).

The analysis of stresses is a complex task due to the complexity of a ship structure. Nowadays the method that is mostly acceptable and spread for analyzing a complex welded structure is the hot-spot stress approach (Petershagen, et al. 1991) based on the effective notch stress approach

(Radaj, 1990). Recommendations for fatigue stress assessment can be found in guidelines prepared by Niemi, (1992, 1995) and Niemi, et al. (2004). Recently new structural approaches were developed by Dong (2001) and Xiao and Yamada (2004).

However, ship welded structures are not perfect and their behaviour depends on a variety of influential factors, namely geometric and material properties, loadings, initial or post built imperfections, deterioration, crack propagation denting etc. The imperfections change permanently the structural capacity of welded structures that initially have been designed to resist loadings, keeping a certain level of safety.

The study presented here deals with a finite element stress analysis of a longitudinally stiffened deck structure, evaluating the hot spot stress distributions and stress concentration factors accounting for different imperfections of a symmetrical welded joint. The hot spot stresses and the stress concentration factors are evaluated at the places adjacent to the trans-verse weld toe. Finite element model uses 20 node solid elements. The hot spot stresses are extrapolated based on the guidelines of the International Institute of Welding developed by Niemi, et al. (2004).

The effect on the hot spot stresses of several imperfections that may occur during shipbuilding, ship repair and during the service life is examined here for symmetrical and unsymmetrical structural joints. They include thickness change misalignment, angular imperfection, rotation of the transverse weld, set of residual deformations that may result due dropped object on deck and a combination of them.

Corrosion and fatigue cracking may be the two most important types of damage in aging ship structures, which lead to surface roughness, reduction of the strength and leakage. Corrosion can be easily inspected and corrosion reduction of plate measured, assessed and consequently plates can be replaced. Due to time constraints, cost considerations, inspection and maintenance are not always performed in accordance with the intentions of the rules and regulations.

However, recently many ships have suffered similar failures and as an example could be mentioned Erika, Castor, Prestige and others.

The most important factor affecting the corrosion rate of the ship hull steel after the coating breakdown (Panayotova, et al. 2004a,b) is seawater temperature. Steel structures corrode at faster rates at higher temperatures than at lower temperatures. As a result, under deck areas and regions adjacent to the engine room or to a hot cargo will tend to corrode faster. Tank top pitting and under deck corrosion can be a serious corrosion problem especially if these areas are left uncoated.

Shipbuilding process involves welding that introduces problems related to the poor heat affected zone (HAZ) toughness. Excessive grain coarsening can lead to cracking in highly restrained joints and thick section material. Inter-granular corrosion can attack the grain boundaries, or immediately adjacent to grain boundaries. This form of corrosion is usually associated with chemical segregation effects or specific phases precipitated on the grain boundaries. Such precipitation can produce zones of reduced corrosion resistance in the immediate vicinity. This problem is often manifested in the heat-affected zones of welds, where the thermal cycle of welding has produced a sensitive structure.

Shipbuilding process involves welding that introduces problems related to the poor heat affected zone (HAZ) toughness. Excessive grain coarsening can lead to cracking in highly restrained joints and thick section material. Inter-granular corrosion can attack the grain boundaries, or immediately adjacent to grain boundaries. This form of corrosion is usually associated with chemical segregation effects or specific phases precipitated on the grain boundaries. Such precipitation can produce zones of reduced corrosion resistance in the immediate vicinity. This problem is often manifested in the heat-affected zones of welds, where the thermal cycle of welding has produced a sensitive structure.

To design and evaluate a marine structure with respect to fatigue damage, the hot spot stress approach is one of the most practical methods and it is usually combined with detailed finite element analysis (Fricke and Petershagen, 1992). It has been noted that the calculated local stress around the structural singularities depends very much on the structural idealization, the element types used and the mesh subdivision. Some application of the approach have been reported by Garbatov, et al. (2002) and Chakarov, et al. (2008).

Normally both fatigue and corrosion will be present and their combined effect needs to be considered in that the decreased net section due to corrosion will increase the stress levels, which in turn in-crease the rate of crack growth. This effect has been considered by Guedes Soares and Garbatov, (1998), which showed that depending on the repair policy adopted one of the two phenomena, would be the dominating one.

Another type of geometrical imperfection that can introduce uncertainty regarding the actual stress concentration factor of a welded joint is the weld shape imperfection is studied by Gaspar et al. (2009).

The effect of non-uniform distributed general corrosion at the back face of the upper deck during ser-vice life of ship on the hot spot stress distribution is studied by Chakarov, et al. (2007). The general corrosion depth is modelled as a non-linear time variant function and a heat affected zone is considered to suffer severe corrosion degradation.

Several studies about estimating high cycle fatigue damage based on spectral approach (HCF) as well as a calculation models for analysis of low cycle fatigue (LCF) have been presented by Guedes Soares et al. (2003), Rudan, and Senjanović, (2005) and Garbatov et al. (2010).

This work deals with the fatigue assessment of marine structures, describing several steps of the calculation accounting for different imperfections, structural degradation and considering the combination of low- and high-frequency induced loading. Fatigue damage is calculated based on the Palgrem-Miner approach.

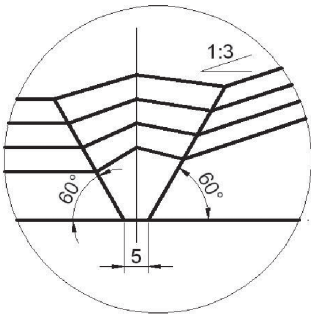

Figure 1. Weld shape for various thicknesses.

2 HOTSPOT STRESS ANALYSIS

This section discus the stress concentration factors of deck structure accounting for several structural imperfections. The studied imperfections are generally present in the stress response characteristics and fatigue damage model applied. Besides commonly present uncertainties in fatigue ship structural analysis associated with structural modelling and the random wave induced loading there are also uncertainties arising from imperfection of structural joint that may occur during manufacturing and the interaction between wave induced load and structure. This work analyses longitudinally stiffened welded decks of a containership based on finite element method and evaluates the hot spot stress distributions and stress concentration factors that result from different types of imperfections. The hot spot stresses and the stress concentration factors are defined at the places alongside to the transverse weld accounting for different imperfections. The analysis deals with the influence of the imperfections over the hot spot stress distribution and not with the reasons for their appearance.

2.1 *Finite element model*

The finite element method is used for determining the structural hot-spot stresses. Based on the results of hot-spot stress analysis the stress concentration factors are determined. The welded joint analyzed here consists of a deck strip with two longitudinals underneath and a girder underneath on each side. The deck strip has a transverse butt joint with a tapered thickness step at half length (see Figure 1).

The finite element analyses applies only the linear static analysis capabilities of commercial software ANSYS, (2009). The stresses and their distributions are influenced by the mesh density and element properties, which requires following some guidelines in predefining of element type, mesh size as well as the stress evaluation at the extrapolation points.

For the structure studied here 20-node elements (Solid95) are used. The Solid95 element is a higher order version of the 3-D 8-node solid element (Solid45). It can tolerate irregular shapes without much loss of accuracy. The Solid95 element has compatible displacement shapes and it is well suited to model curved surfaces. The element is defined by 20 nodes having three degrees of freedom per node: translation in the nodal *u, v* and *w* directions. The Solid 95 element has plasticity, creep, stress stiffening, large deflection and large strain capabilities.

Additionally to the Solid 95 element, 8 node shell elements (Shell93) are also used and the results obtained are compared.

Several requirements have to be satisfied for performing acceptable calculations related to discontinuities in the vicinity and the stress gradient close to the hot spot. However, the 20 node solid elements used for finite element modelling and the stresses obtained at midpoints of the first elements are normally slightly exaggerated due to the singularity at the weld toe and latter are somehow corrected by linear extrapolation applied for defining the hot-spot stresses.

A uniaxial constant stress at the left end cross section is applied, where the thinner deck strip plate is located. All right and left end cross section nodes are fixed in the vertical (*w*) direction. All the right end cross section nodes are fixed in the longitudinal (*u*) direction and about the transverse (*v*) and vertical (*w*) directions.

The mesh pattern of hot spots is designed in such a way that the actual hot-spot can be analyzed, and the structural stresses can be determined by extrapolation. In the case when a plate subjected to uniaxial membrane stress and the two welded deck plate have the same thickness, the location of the hot-spot is obvious.

2.2 *Hot spot stress analysis of symmetrical joint*

To define the stress distribution around the hot spots a specific modeling technique is applied here.

The analysis is based on direct stress calculation where the finite element mesh is generated in such way that a relatively rough one is used for the zones away from the hot spot and a fine mesh of size t*t is generated around the analyzed hot spots.

The critical hot spots are expected to appear on the side of the thinner plate, where the weld toe is located on the plate surface. The welded structure is subjected to uniformly distributed tensile stresses. Rectangular strips of $t*t$ elements size are used around the weld, while larger elements are used away from the weld toe to mesh the rest of the models.

Based on $\sigma_{HS} = 1.5\sigma_{0.5t} - 0.5\sigma_{1.5t}$ linear stress extrapolation is performed for the hot spot stresses. The hot spot stresses and stress concentration factors are estimated based on the maximum principal stress at the weld toe line of the thinner plate.

2.2.1 *Stress concentration factor as a function of thickness change misalignment*

A model consists of a deck strip with two longitudinals underneath and a girder underneath on each side (see Figure 2).

The peaks of the hot spot stresses along the path move with changing of the step thickness change ratio. For small difference between the thicknesses the stresses distribution between longitudinals have smooth parabolic shape, but with increasing the differences of the thickness, the peaks become close to the longitudinals as the stresses are lower between them.

The peaks in stresses along the longitudinals underneath are more clearly marked at large difference between plate's thicknesses, and less visible with decreasing of this difference. The stress concentration factors as a function of step thickness changes are presented in Figure 3, where contour plots are created by fitting a 3D surface function to a 3D scatter plot.

2.2.2 *Stress concentration factor as a function of angular imperfection*

During the shipbuilding and ship repair process, welded plates cannot be perfectly aligned accordingly to design plans because of different causes. This possible misalignment is modelled here as an angular imperfection. The effect of this imperfection to hot spot stress distributions and resulting stress concentration factors is studied based on the calculation of hot spot stresses as a function of the angle that is formed between plates and perfect horizontal plane. The angular misalignment results in a displacement of the plate's edges in the w -direction, assumed to be "+w" when the plate's edges move up, and "–w" when the plate's edges move down.

It can be observed from Figure 4 that the stresses distribution along the paths 0.5t and 1.5t as for example when $w = \pm 0.5$ m are much bigger in the case, when the plate's edges are upward than in the case when the plates edges are down-ward. This effect is magnified by accounting for the step thickness changes that introduce additional eccentricity and additional bending moment.

The stress concentration factor as a function of plate thickness and for both moving up and down of the plates edges is shown in Figures 5 and 6. It can be noted that bigger differences between plate thicknesses correspond to bigger stress concentration factor.

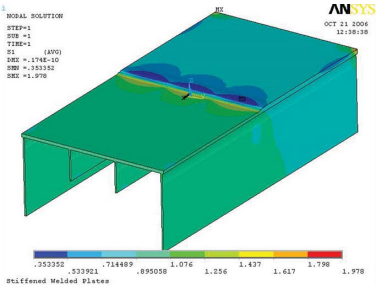

Figure 2. Model geometry and principal stress distribution.

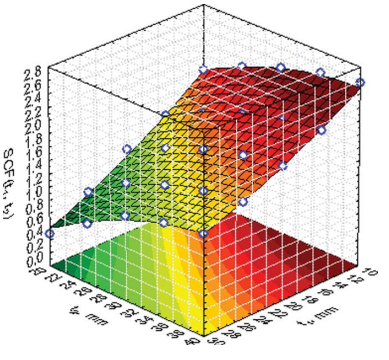

Figure 3. SCF as a function of thickness misalignment.

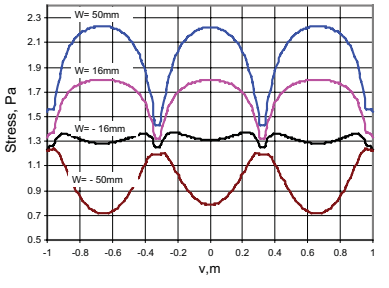

Figure 4. Stresses along the path, 0.5 t for $t_1 = 20$ mm, $t_2 = 30$ mm and various w.

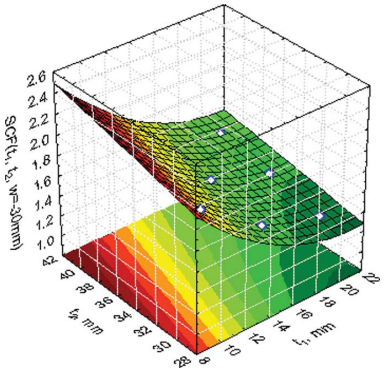

Figure 5. SCF for angular imperfection, $w = -30$ mm.

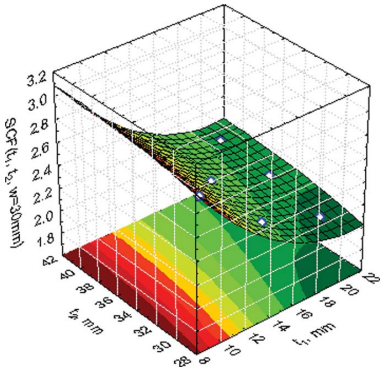

Figure 6. SCF for angular imperfection, $w = +30$ mm.

2.2.3 *Stress concentration factor as a function of rotation of transverse weld toe*

The rotation of the transverse weld toe is modelled by a u displacement of the weld toe in the x-direction. The rotation of the weld toe that is examined here varies in the interval from $u = 4$ mm to $u = 50$ mm (from 0.230 to 2.860).

The stress concentration factor as a function of t_1 and t_2 for $u = 30$ mm is given in Figure 7. It is observed the effect of weld toe rotation for different angles studied here has insignificant importance to stress concentration factor calculation.

2.2.4 *Stress concentration factor as a function of residual deformations*

Several locations of residual deformations settled on the thinner plate are examined as can be seen in Figure 9. The residual deformation is modelled by a triangular shape. This type of shape is defined based on the idea that it can be a result of a dropped container on deck, hitting the plate with a corner.

The stress concentration factor calculated for the locations 1 as a function of t_1, t_2 is shown in Figure 10.

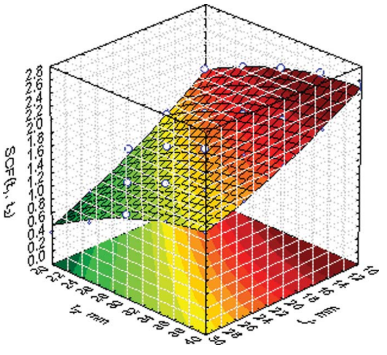

Figure 7. SCF for angular imperfection, $u = 30$ mm.

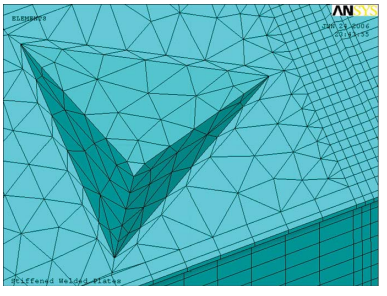

Figure 8. Shape of residual deformation.

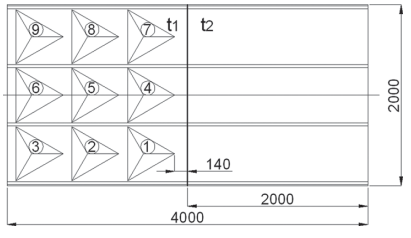

Figure 9. Locations of residual deformations.

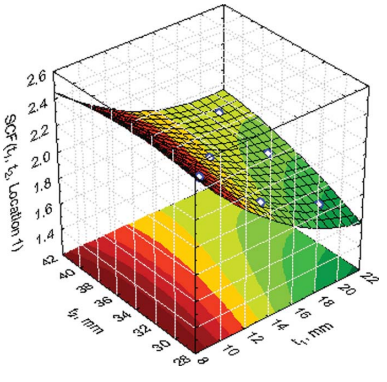

Figure 10. SCF as a function of t_1, t_2 for the location 1.

It has been observed that the stress concentration factor has a maximum when the deformation is located near the lateral edge of the thinner plate or in the middle, the locations 1 and 4.

3 EFFECT OF WELD SHAPE IMPERFECTIONS

The effects on the stress concentration factor of geometrical imperfections related to misalignments in structural joints were analysed in Section 2. Another type of geometrical imperfection that can introduce uncertainty regarding the actual stress concentration factor of a welded joint is the weld shape imperfection. This type of imperfection results from the welding process and therefore it is always present in a welded joint. Because of its random nature a stochastic approach has to be adopted to quantify its effect on the stress concentration factor.

In this chapter the effect of this type of geometrical imperfection on the structural hot-spot stress distribution is analysed. The containership's deck structure presented in Section 2 is used as case study. The finite element analysis method is used to calculate the stress distribution in the vicinity of the weld toe, assuming that only weld shape imperfections are present in the welded joint. The finite element model and the linear extrapolation scheme used in Section 2 to calculate the hot-spot stresses are adopted for this study. The weld shape imperfections are simulated using a Monte Carlo procedure with weld profile parameters defined as random variables. Five levels of weld shape imperfection (e.g., associated with the quality levels of welding) are simulated and its effect on the stress concentration factor is assessed using fitted probability distributions and regression analyses.

3.1 *Finite element model*

The finite element model presented in Section 2 was adopted for this study as well as the ANSYS (2009) finite element code. However, specific modelling and analysis techniques were used due to the type of imperfection considered and the approach adopted to quantify its effect on the hot-spot stress distribution. The finite element code was coupled with a Monte Carlo simulation code in order to generate random samples of imperfect weld shapes and compute the hot-spot stress distribution correspondent to each imperfect weld shape generated. This can be performed using the batch-mode capabilities of the finite element code and input files in ANSYS Parametric Design Language (APDL).

The focus in this study was the finite element modelling of the transverse butt-weld with random geometrical imperfections. The modelling was performed in two steps within the Monte Carlo simulation procedure. First, a perfect geometry is generated considering the weld shape defined by two flat surfaces in the solid model, as represented in Figure 11. This idealization of the weld shape is commonly adopted for the hot-spot stress approach (Niemi et al. 2004). Afterwards, the finite element mesh is generated and the positions of the corner nodes represented in Figure 11 are modified along the transverse weld accordingly to random deviations sampled by the Monte Carlo procedure. The positions of the midside nodes of the 20-node solid finite element Solid95 are also adjusted. The corrected positions are defined by the midpoint of the modified element's edges. The stochastic model adopted for the weld shape random imperfections is discussed in the next section as well as more details of its implementation in the finite element model.

The finite element mesh is generated using an approach similar to the one used in the study presented in Section 2.

The loading and the boundary conditions are identical to the ones used in the study presented in Chapter 2.

3.2 *Stochastic modelling of the weld shape imperfections*

The weld shape imperfections are modelled as random deviations in the vertical position of a mesh of equally spaced reference points positioned along the weld toe and along the weld face edge, as shown in Figure 12. These reference points are

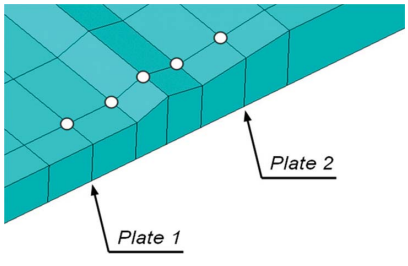

Figure 11. Idealised geometry of the butt-weld profile.

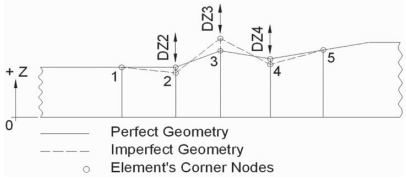

Figure 12. Longitudinal cross-section of the butt-welded joint.

defined in the simulation as being the corner nodes of the finite element mesh on the weld toe and weld face edge lines. For convenience, these nodes are now designated as reference nodes.

The convention adopted for the reference nodes numbering and vertical position, for perfect and imperfect geometries or weld shapes, are shown in Figure 13. This convention was used to derive the formulation that describes the vertical position of the reference nodes in the Monte Carlo simulation of the weld shapes. As shown in Figure 13, the weld shapes simulation is performed considering that the reference nodes 1 and 5 are fixed, and that the positions of the reference nodes 2 to 4 describe the weld profile along the butt weld for perfect and imperfect weld shapes. The vertical position of these reference nodes is given by,

$$Z_i^I = Z_i^P + Z_i^D \tag{1}$$

with $i = 2$ to 4 the reference node index.

According to Eqn. 1, the vertical coordinates for imperfect weld shapes Z_i^I are given by the vertical coordinates for perfect weld shapes Z_i^P affected by random vertical deviations Z_i^D. For perfect weld shapes the vertical coordinates of the reference nodes can be easily obtained from the structural detail geometric parameters. It should be noted that the perfect weld shape is an idealization used in this study as reference geometry for weld shapes' simulation purposes, since it is not possible in practice to reproduce such geometry because of the imperfections induced by the welding process.

The vertical random deviations Z_i^D are given by a multivariate normal distribution. This probabilistic model is widely known and can be found in the literature about statistics or reliability, as for example in Melchers, (1999). This distribution is given by:

$$f_Z(z) = (2\pi)^{-N/2} |C_Z|^{-1/2} \times \exp\left[-\frac{1}{2} (z - \mu_Z)^T C_Z^{-1} (z - \mu_Z) \right] \tag{2}$$

where N is the dimension of the distribution, Z the vector of random variables, μ_Z the vector of mean values and C_Z the covariance matrix of the random vector Z. The simulation was performed considering the dimension N equal to three, since the weld profiles are defined by the vertical coordinates of the three reference nodes {2, 3, 4} in Figure 13. The random deviations Z_i^D are positive or negative increments in the vertical position of the reference nodes, considering that they are measured from the perfect geometry and have zero mean value μ_Z. The covariance matrix C_Z can be written as a function of the correlation coefficients and standard deviations of the random variables, as known from statistics. The standard deviation σ_i of each random variable is defined by the coefficient of variation COV_i, considering as mean value μ_i the vertical coordinate Z_i^P in the perfect geometry. The coefficients of variation are defined using the same value for all random variables, i.e. $COV_i = \delta$ with $i = 2$ to 4. This parameter is used as a global measure of the magnitude of the weld shape imperfections.

The correlation coefficients ρ_{ij} are defined, assuming that the random deviations in the vertical position of the reference nodes 2 and 4 are independent, which means that $\rho_{24} = \rho_{42} = 0$. The correlation between the vertical deviations in the weld face node and weld toe nodes, described by the coefficients $\rho_{23} = \rho_{32}$ and $\rho_{34} = \rho_{43}$, may be high, because of the welding processes' characteristics, i.e. correlations of 0.70 and even higher may have to be used in the simulation.

The random deviations are defined by the probabilistic model given by Eqn. 2 with the proposed procedure to define the covariance matrix. However, generating random vectors according to a multivariate distribution is usually a difficult task. There are methods in the literature that may be used to perform this simulation, most of them often applied in reliability calculations (Melchers, 1999). In the simulation performed in this study, the random vectors were generated using a subroutine available in a numerical library for statistical applications that generates pseudo-random vectors

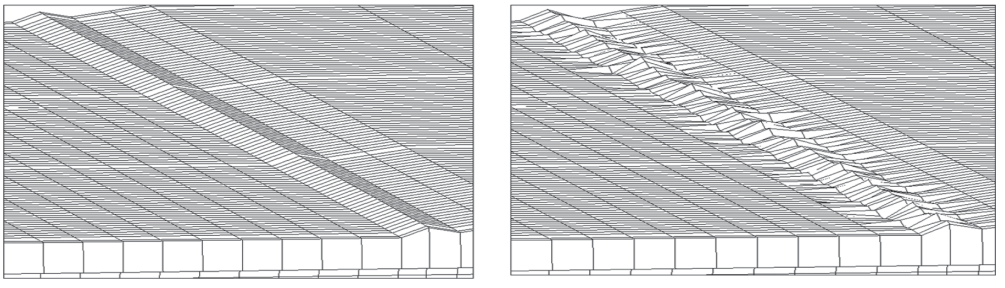

Figure 13. Weld shape for each imperfection level considered: perfect case and imperfection level IL 5.

from a multivariate normal distribution (IMSL, 1997). The numerical procedure adopted in this subroutine can be found in the numerical library.

The Monte Carlo simulation of the imperfect weld shapes is performed according to the previous procedure, in which a random vector is generated for each set of reference nodes. It is assumed that the random deviations along the butt weld direction are independent, i.e. the random deviations of a set of reference nodes with $y = y_1$ are independent of the random deviations of a set of reference nodes with $y = y_2$, where y is the transversal coordinate aligned with the butt weld and $y_1 \neq y_2$. This assumption is reasonable because the transversal distance between adjacent nodes is equal to the plate thickness.

The modelling of the imperfect weld shapes in the finite element model is made according to the previous procedure, using the simulated random deviations to adjust the vertical position of the reference nodes, as shown in Figure 12. Examples of imperfect weld shapes simulated with different values of the parameter δ used as a global measure of the level of imperfection are presented in Figure 13. The perfect weld shape is presented for comparison purposes, since it is not representative of real weld shapes. As expected, the magnitude of the weld shape imperfections increases with the parameter δ. The statistical description of the weld shapes as a function of this parameter is presented next.

3.3 *Statistical description of the weld shape as a function of the imperfection level*

The simulation of the imperfect weld shapes can be performed with any reasonable value defined for the parameter δ. This parameter is used to define the magnitude of the weld shape random imperfections; however, it does not allow by itself an easy interpretation of the weld shapes, as there is no direct relation between this parameter and geometrical parameters that can be used to describe the weld profile. Thus, it is important to quantify the imperfect weld shapes generated with a range of δ values by geometrical parameters usually applied in practice to characterize the weld profile. These parameters can be found in guidelines related to shipbuilding and repair quality standards, as for example in IACS, (2006). According to this quality standard, there are three main parameters for this welded joint: (1) the weld face height, H; (2) the weld toe angle, θ; and (3) the weld toe position, related to the weld undercut, D. These three geometrical parameters were used to quantify statistically five random samples of imperfect weld shapes, each of which corresponding to a different value of the parameter δ. In the present study the values considered were all integers in the interval [1, 5] representing the parameter δ in percentage, which define five classes of weld shapes, designated from now on as imperfection levels for convenience, because they are related to different quality levels of the welding process.

For each imperfection level, 100 simulations of imperfect weld shapes were performed, obtaining for each simulation one random sample with 197 random vectors with coordinates of the weld profile reference nodes, as the number of nodes in the transversal direction of the finite element mesh is 197. For each imperfection level, the 100 random samples were combined and the three geometrical parameters $\{H, \theta, D\}$ calculated afterwards. The sample statistics of these three parameters for the five imperfection levels considered are presented next by histograms, fitted probability distributions and tolerance intervals.

It was concluded that the random deviations in the three parameters are normally distributed with zero mean, as can be seen in Figure 14, where the histograms and the fitted probability distributions are shown for the imperfection level three as example. This conclusion was expected since the random deviations in the vertical position of the weld profile reference nodes are generated according to a normal distribution.

Parameters of the fitted probability distributions are given in Tables 1 to 3 for each imperfection level considered. The tolerance intervals presented for the three geometrical parameters were calculated considering 95% of the weld profile population and assuming the same percentage for the confidence level. These parameters are easily interpreted; however, the definition adopted for the weld toe angle should be clarified. This parameter was defined as the angle between the tangent to the plate surface and the tangent to the weld face, both evaluated at the weld toe. The deviations referred in the sample statistics are measured in relation to the perfect weld shape.

The Effect of the weld shape imperfections on the stress concentration factor.

The analysis of the effect of the weld shape imperfections on the structural hot-spot stresses was carried out using the Monte Carlo simulation

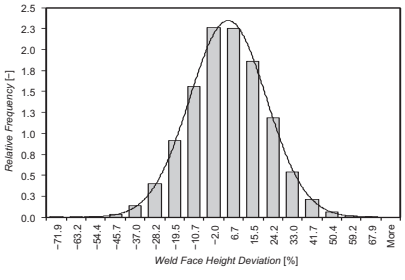

Figure 14. Distribution of weld face height, H, IL 3.

Table 1. Tolerance intervals for weld face height.

Imperfection level		1	2	3	4	5
μ	(*mm*)	0.000	0.000	0.000	0.000	0.000
σ	(*mm*)	0.281	0.561	0.847	1.130	1.411
H_-	(*mm*)	–0.6	–1.1	–1.7	–2.2	–2.8
	(%)	–11.1	–22.1	–33.3	–44.5	–55.5
H_+	(*mm*)	0.6	1.1	1.7	2.2	2.8
	(%)	11.1	22.1	33.3	44.5	55.5
ΔH	(*mm*)	1.1	2.2	3.3	4.4	5.5
	(%)	22.1	44.2	66.7	89.0	111.1

Note: Tolerance interval for 95% of the weld profile population with 95% confidence.

Table 2. Tolerance intervals for weld toe angle.

Imperfection level		1	2	3	4	5
μ	(Deg.)	0.000	0.000	0.000	0.000	0.000
σ	(Deg.)	1.641	3.293	4.952	6.601	8.163
θ_-	(Deg.)	–3.2	–6.5	–9.7	–12.9	–16.0
	(%)	–2.1	–4.1	–6.2	–8.3	–10.3
θ_+	(Deg.)	3.2	6.5	9.7	12.9	16.0
	(%)	2.1	4.1	6.2	8.3	10.3
$\Delta\theta$	(Deg.)	6.4	12.9	19.4	25.9	32.0
	(%)	4.1	8.3	12.5	16.6	20.6

Note: Tolerance interval for 95% of the weld profile population with 95% confidence.

Table 3. Tolerance intervals for weld toe position.

Imperfection level		1	2	3	4	5
μ	(*mm*)	0.000	0.000	0.000	0.000	0.000
σ	(*mm*)	0.232	0.463	0.697	0.934	1.157
D_-	(*mm*)	–0.5	–0.9	–1.4	–1.8	–2.3
	(%)	–2.3	–4.5	–6.8	–9.2	–11.3
D_+	(*mm*)	0.5	0.9	1.4	1.8	2.3
	(%)	2.3	4.5	6.8	9.2	11.3
ΔD	(*mm*)	0.9	1.8	2.7	3.7	4.5
	(%)	4.5	9.1	13.7	18.3	22.7

Note: Tolerance interval for 95% of the weld profile population with 95% confidence.

procedure. For each imperfection level considered, 1000 simulations were performed, obtaining for each case the structural hot-spot stress distribution along the weld toe line. Based on these stress distributions, samples of maximum structural hot-spot stress were obtained for each imperfection level. For convenience, these stresses are presented as stress concentration factor (SCF) normalized by the value obtained for the perfect case, i.e. normalized by the SCF that is obtained if the weld shape is considered perfect. For this reference case the value obtained was $K_p = 1.613$. The sample statistics of this parameter for the five imperfection levels considered are presented next by histograms, fitted probability distributions and tolerance intervals.

Figure 15 presents histograms and fitted probability distributions to the simulation results for the five imperfection levels. The histograms show that the results obtained for the SCF may be described by a log-normal probability distribution or, for some imperfection levels, by a normal probability distribution. The best distribution to describe the simulation results was selected using probability paper plots and Kolmogorov-Smirnov goodness-of-fit tests.

It was concluded that the log-normal distribution is more appropriate than the normal distribution, as it can describe the simulation results for the five imperfection levels considered with better results in the Kolmogorov-Smirnov goodness-of-fit test, where a 5% significance level was adopted. The parameters of the fitted log-normal distributions are given in Table 4. shows the fitted probability density functions for the five imperfection levels.

The effect of the weld shape imperfections on the SCF is given in Figure 16. This figure shows the sample values of normalized SCF obtained with the simulations performed. The tolerance intervals were calculated considering 95% of the weld profile population and assuming the same percentage for the confidence level. The tolerance limits are given in Table 4 as a function of the imperfection level parameter, in absolute values as well as in relation to the mean values.

Simple linear regression analyses were carried out to find suitable first- and second-order polynomial functions that may be used to describe the mean value and the tolerance limits as a function of the imperfection level. Based on these analyses, it was concluded that these parameters increase with the imperfection level parameter δ. The increase is linear for the mean value and quadratic for the upper and lower tolerance limits, as can be seen in Figure 16 The distance between the upper and lower tolerance limits tends to increase because of the increase in the variability of the simulation results, which reflects the effect of the weld shape random imperfections on the maximum structural hot-spot stress.

The regression coefficients as well as the coefficients of determination R^2 obtained for each case are given in Table 5.

In Table 5 the imperfection level parameter is denoted by δ (i.e. coefficient of variation COV_i in percentage) and the regression coefficients associated with the quadratic, linear and constant terms

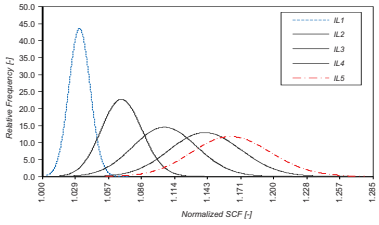

Figure 15. Distributions of normalized stress concentration factor (SCF) as a function of the imperfection level.

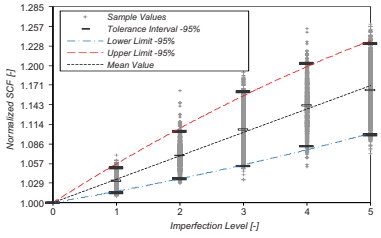

Figure 16. Effect of the weld shape imperfection level on the normalized SCF.

Table 4. Distribution parameters and tolerance intervals for normalized SCF as a function of the imperfection level.

Imperfection level		1	2	3	4	5
λ	-	0.032	0.066	0.101	0.132	0.151
ξ	-	0.009	0.016	0.025	0.027	0.029
K_-	-	1.015	1.035	1.053	1.082	1.099
	(%)	–1.7	–3.2	–4.8	–5.2	–5.6
K_+	-	1.050	1.104	1.161	1.203	1.232
	(%)	1.7	3.3	5.0	5.4	5.8
ΔK	-	0.036	0.069	0.108	0.121	0.133
	(%)	3.5	6.4	9.8	10.6	11.4

Note: Tolerance interval for 95% of the weld profile population with 95% confidence.

Table 5. Regression coefficients for mean values and tolerance limits of normalized stress concentration factor (SCF).

	δ^2	δ	1	R^2
K_+ / K_P	–2.34E-03	5.89E-02	1.00	0.997
K_0 / K_P	0.00	3.40E-02	1.00	0.996
K_- / K_P	9.22E-04	1.56E-02	1.00	0.995

Note: Normalization factor, $K_P = 1.613$.

of the polynomials are identified by the order of this parameter in the first line of the table.

The results obtained show that SCF increases considerably with the level of weld shape imperfections. As a numerical example, if a moderate level of imperfection is assumed and the 95% upper limit polynomial is considered to describe the simulation results, the increase in the SCF may be 15.6% compared with the value obtained if a perfect weld shape is considered. For further fatigue damage assessment the notch effect of the weld toe need to be included.

4 HOTSPOT STRESS ANALYSIS ACCOUNTING FOR CORROSION DETERIORATION

This section analyses the hot spot stress distributions and stress concentration factors of longitudinally stiffened welded deck joints subjected to corrosion and fatigue. The stress concentration factors are defined at the alongside to the transverse welds accounting for the presence of locally non uniform distributed corrosion. Several stages of structural deterioration due to corrosion are evaluated and the correlation between the status of degradation and stress concentration factor are established.

The finite element method is used to analyze the structural hot spot stresses. Based on the results of hot spot stress calculation the stress concentration factors are determined and further fatigue life can be estimated.

The welded joint analyzed here is the same with the one analyzed in Section 2 and has been used the same approach to analyze the hot-spot stress distribution.

For the needs of the present study a corrosion depth is distributed so as to account for the presence of the heat affected zone and inter-granular corrosion. The general corrosion reduces uniformly the thickness of the under deck structural longitudinal and transverse members, while the corrosion depth of deck plate is developed in a function of time, combining general and inter-granular corrosion. The general corrosion deterioration is modelled based on the model of Guedes Soares and Garbatov, (1999).

The model is based on the solution of a differential equation of the corrosion wastage that leads to the followings:

$$d(T) = d_\infty \left(1 - e^{-\frac{T-\tau_C}{\tau_T}} \right), T > \tau_C$$

$$d(T) = 0, T \le \tau_C$$

where d_∞ is the long- corrosion wastage, $d(T)$ is the corrosion depth at time T, τ_c is the time without corrosion which corresponds to the start of failure of the corrosion protection coating (when there is one), and τ_T is the transition time duration.

The principal characteristics of corrosion depth as a function of time for under deck longitudinals, transfer frames and plates are $d_\infty = 6$ mm, $\tau_c = 10$ years and $\tau_T = 5$ years and for HAZ are $d_\infty = 12$ mm, $\tau_c = 10$ years and $\tau_T = 5$ years respectively (see Figure 17). It has to be pointed out that the coating life for the deck structure is taken as $\tau_c = 10$ years that in many satiation could be considered reasonable due to the fact that the structural components are exposed to the same environmental conditions.

The corrosion depth distribution function around deck plate can be seen in Figures 18 and 26. The shape and the residual deck thickness changes are given as a function of time.

In order to obtain the stress distribution in the thinner plate near the weld, where the maximum value are expected, several paths on the top of the plate have been examined. Two of them, situated $0.5t$ and $1.5t$ away from the weld toe and necessarily for the linear stress extrapolation are parallel of the weld. The third one is transversely of the weld situated in the plain of symmetry of the model.

The principal stress distribution along the weld toe can be seen in Figure 19. It can be noted a significant stress elevation around the weld toe. There is also a stress elevation around the HAZ.

Figure 20 shows the stress distribution along a path perpendicular of the weld toe (see the path in Figure 19). It can be observed that in the places, where the plate thickness is reduced due to local corrosion, the principal stresses are reduced in some zones, as there is increasing of the stresses around others, which is different with respect to the plates that are subjected to uniformly distributed corrosion deterioration. The principal stresses are higher in the area close to the transverse weld, as smoothly de-crease with moving away.

The peaks in the principal stresses along the path are more clearly marked with increasing of the ship's age, as is shown in Figure 21 for the paths $0.5t$ and $1.5t$ at 40th year, and in Figure 22 along the path, $0.5t$ for various years. The peaks of the stresses between longitudinals are flat for intact plate, pass through parabola and become sharp at the end of the service life of the ship structure. As can be seen from Figure 23, the SCF smoothly increases with corrosion deterioration of plate thickness during the service life of the ship.

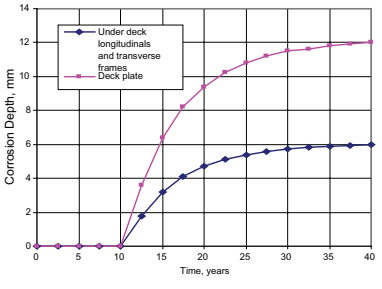

Figure 17. Corrosion depth as a function of time.

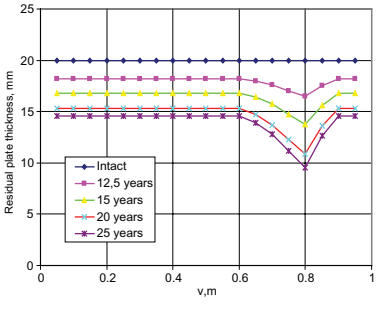

Figure 18. Residual plate thicknesses.

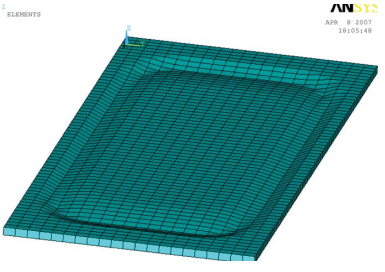

Figure 19. Corrosion depth distribution around the deck plate.

Figure 20. Principal stress distribution around the weld toe, path perpendicular to the weld toe.

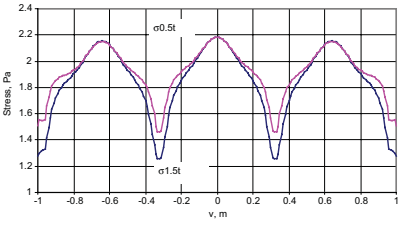

Figure 21. Stresses distribution along the paths $0.5t$ and $1.5t$, $t = 40$ years.

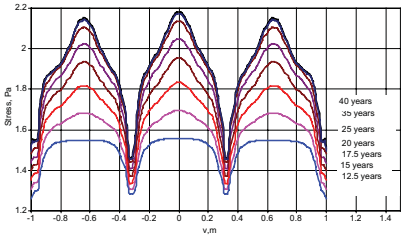

Figure 22. Stresses distribution along the path 0.5*t*.

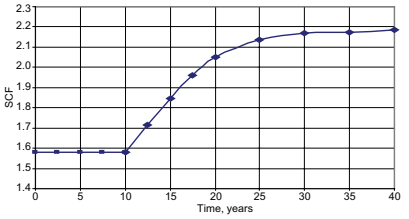

Figure 23. SCF as a function of time.

5 FATIGUE DAMAGE ASSESSMENT BASED ON SPECTRAL APPROACH

This section presents direct calculation model for estimating high cycle fatigue based on spectral approach (HCF) as well as a simplified calculation models for analysis of low cycle fatigue (LCF) and the combination of the two.

5.1 *High cycle fatigue damage*

In shipbuilding industry HCF is commonly investigated using probabilistic methods in combination with hydrodynamic and structural analysis, with different simplifications. Several classification societies established Rules for HCF analysis and the procedures proposed are to be followed whenever possible. In this way uncertainties and spreading of the results will be minimized.

Fracture analysis of crack growth is usually not of main concern as cracks appear on various and rather unpredictable locations in structural details. Therefore, HCF analysis aims to determine the fatigue life of a structural detail prior to crack. In addition, the cracks in ship structures may sometimes grow for meters in length before becoming a threat to the ship integrity.

HCF of structural details occurs due to a high number of loading cycles of moderate amplitude, typically in a range of 10^4 to 10^8 cycles. Ships in service are exposed to a number of loads that vary in time, such as wave loads, vibrations, thermal stresses etc. Among these, wave loads are considered to be the main cause of high cycle fatigue for structural details directly exposed to wave loads (e.g. side shell longitudinals), but also for a number of other structural details that "feel" the wave induced hull structure deformation. Some types of ships like i.e. fast ferries are exposed to a variety of different loads inducing fatigue, each contributing to a total fatigue accumulation.

Structural details life-span is commonly estimated by fatigue damage calculation based on S-N approach. Two main groups of standard S-N curves are UK DEn (HSE) and IIW S-N curves (IIW, 1995) covering a range of structural details in classes and categories.

Although S-N curves are being recognized as the industry standard, they are not always easily applicable to problems in shipbuilding industry. They are hardly able to take into account a variety of structural details found in ship structures and also they do not address the corrosion environment issues directly. Due to that certain Classification societies define universal S-N curves that are applicable to any type of structural details both in aggressive and non-aggressive environment (DNV, 2008). For example, DNV defines four universal S-N curves: S-N I for welded joints in air or with cathode protection against corrosion, S-N II for welded joints in corrosive environment and, in the similar manner, S-N III and S-N IV curves for base material.

In its simplest form, when the structural load is of constant amplitude, the number of cycles till failure N for a given stress range $\Delta\sigma$ may be determined directly from S-N curve at a single point $(\Delta\sigma,N)$ or using analytical expression for S-N curve:

$$N = \bar{a}\Delta\sigma^{-m}$$

where $\bar{a}$ and m are S-N curve parameters.

If the amplitude varies, a long-term distribution of stress ranges may be divided approximately in blocks (intervals) of constant stress range. Then particular damage is calculated for a number of cycles for each block and total damage according to Palmgren-Miner summation rule.

Due to complexity of ocean waves the stress range cycles on the oceangoing vessels are considered to be distributed by the probability density function $f(\Delta\sigma)$. Since a structural detail is exposed to n_0 stress cycles during its lifetime it follows that a number of cycles for each stress range interval $[\Delta\sigma,\ \Delta\sigma + d\Delta\sigma]$ is equal to $n_0\ f(\Delta\sigma)d\Delta\sigma$ and the fatigue damage may be calculated as:

$$D = \int_0^\infty \frac{n_0 f(\Delta\sigma)}{N(\Delta\sigma)} d\Delta\sigma$$

where $N(\Delta\sigma)$ is a number of cycles till failure at constant stress range $\Delta\sigma$.

HCF spectral analysis aims to take into account most effects that contribute to fatigue damage accumulation in structural details on the ocean-going vessels such as sailing route, loading condition, sea state (wave spectra) etc.

Spectral HCF analysis consists of four steps:

a. hydrodynamic analysis, where wave loads are calculated for different combinations of wave lengths and heading angles, ship speed and ship loading conditions;
b. structural analysis, where ship structure is subjected to hydrodynamic loads;
c. statistic and stochastic analysis, where stress transfer functions are combined with particular sea-state occurrence probability and so the long-term stress range distribution is evaluated;
d. fatigue damage calculation.

The aim of hydrodynamic analysis is to evaluate regular wave loads acting on the ship: wave induced pressure distribution on the ship hull and inertial forces due to global ship motions (accelerations of the masses). Internal pressure loads in cargo tanks may be evaluated as well. Linear modelling of the ship response is considered sufficient for fatigue assessment purposes. Hydrodynamic calculations based on both strip and sink-source panel theory may be performed.

Hydrodynamic calculations need to take into account full and ballast loading conditions and a set of wave lengths (of unit amplitude) and wave headings that ship will be exposed to during her service. The length of the model should extend at least over L_{pp}. The masses should be modelled realistically and ship speed during service, both in full and ballast loading condition, needs to be taken into account. DNV recommends 2/3 of the actual ship service speed to be used for calculation. The procedure is also applicable to non-moving vessels such as FPSO.

A sufficient number of wave periods and headings are to be used for determining regular wave transfer functions. All wave headings have to be taken into account and for each a minimum of 20 to 25 wave periods shall be included in the calculation. This may easily induce several hundred load cases that are to be analyzed.

Once the hydrodynamic loads are defined, both in real and imaginary domain, they are transferred to structural model and then structural FE analysis is performed. The transfer of the hydrodynamic loads is normally performed automatically by the software. If only a part of ship structure is modelled (i.e. three cargo hold in the amidships) than the adequate sectional forces and moments are to be applied on the model ends. Particular "umbrella" structure may be assembled with light and stiff beam elements connecting models end to a single node that will induce vertical bending moment to the structure.

For each structural detail of concern a hot spot (or notch) stress range transfer functions $|H_\sigma(\omega, \vartheta)|$ are to be determined.

The elevation of the ocean surface is a highly irregular and random process. However, irregular waves may be mathematically modelled as a linear combination of a number of regular waves with different wave heights, wave periods and random phase angles, which allows the ocean surface to be described as a stochastic process. The joint distribution of wave heights and wave periods for short-term sea states is available for different geographic Mardsen zones.

Within a short time interval the fully developed ocean wave height (or surface pattern) becomes a stationary, narrow-banded random process. Wave peaks are therefore assumed to follow a Rayleigh distribution. Commonly a Pierson-Moskowitz wave spectrum is used to describe short-term sea state:

$$S_\eta(\omega, H_Z, T_z) = \frac{H_Z^2}{4\pi}\left(\frac{2\pi}{T_Z}\right)^2 \omega^{-5} \times \exp\left(-\frac{1}{\pi}\left(\frac{2\pi}{T_Z}\right)^4 \omega^{-4}\right)$$

Assuming a linear model, for each sea state a response spectrum will be directly determined from the hot spot stress range transfer functions and wave spectrum:

$$S_\sigma(\omega, H_Z, T_Z) = |H_\sigma(\omega, \vartheta)|\, S_\eta(\omega, H_Z, T_Z)$$

The response spectrum will be assumed as a stationary, narrow-banded random process. Therefore, response peaks (stresses and corresponding stress ranges) are Rayleigh distributed:

$$F_{\Delta\sigma ij}(\sigma) = 1 - \exp\left(\frac{-\sigma^2}{8m_{0ij}}\right)$$

where m_0 is spectral moment of the order zero.

A cumulative distribution of the long-term response may be calculated as a weighted sum over all sea states and headings. The long-term distribution is therefore:

$$F_{\Delta\sigma}(\sigma) = \sum_{\substack{i=1 \\ j=1}}^{\substack{\text{all seastates} \\ \text{all heading}}} r_{ij} \cdot F_{\Delta\sigma ij}(\sigma) \cdot p_{ij}$$

where p_{ij} is the probability of occurrence of a given sea state i combined with heading j and r_{ij} is the ration between the response crossing rates in a given state and the average crossing rate.

The sum of Rayleigh distributions may be fitted by Weibull distribution that is described with two parameters, shape parameter h and scale parameter q:

$$F_{\Delta\sigma}(\sigma) = 1 - \exp\left(-\left(\frac{\sigma}{q}\right)^{h}\right)$$

Finally, fatigue damage may be calculated by the resulting expression for high cycle fatigue damage summation according to (DnV, 2008):

$$D_{HCF} = \frac{T_d}{T_0 \cdot \bar{a}} p_n q_n^m \Gamma\left(1 + \frac{m}{h_n}\right)$$

where D_{HCF} is high cycle fatigue damage, $\bar{a}$ and m are S-N curve parameters, T_d is design life of ship in seconds, T_0 is long-term average response zero-crossing period, p_n is fraction of design life in loading condition n, and q_n and h_n are the Weibull distribution stress range scale and shape parameters, respectively, for each loading condition n.

Highly stressed structural details are prone to low cycle fatigue (LCF), when the fatigue of material occurs after 10 to 10^4 cycles. Although the Classification societies verify structural details against fatigue for the entire service life. However, often fatigue damage occurs much earlier, leading to costly ship repairs. LCF will occur at locations where micro fractures exist, at the weld root notches or any other location where local stress is very high and higher than yield stress at times.

LCF in ship structures is only recently being investigated for example by Urm et al. (2004) and Heo et al. (2004).

Currently, LCF calculation methods may fit in one of the two groups: methods using range of local deformations and methods of pseudo-elastic stresses. The method of local deformations aims to define the deformation and stresses at highly stressed micro-locations as a function of global deformation and stresses of structural details. Figure 29 shows the relation between elastic global behaviour of structural detail and elastic-plastic local behaviour of crack tip at micro-location.

The global elastic behaviour affects the local elastic-plastic behaviour in a way that the local stress-deformation curve is formed in a shape of hysteresis. If the material behaves in a stable manner, after a number of cycles the shape of hysteresis doesn't undergo any further changes and then all the points on hysteresis satisfy Ramberg-Osgood equation:

$$\varepsilon_{loc} = \frac{\sigma_{loc}}{E'} + \left(\frac{\sigma_{loc}}{K'}\right)^{1/n'}$$

where σ_{loc} and ε_{loc} are local stress and strain, respectively, E' is the stable cyclic Young's modulus of elasticity, K' is a strength coefficient and n' is a strain hardening exponent. By replacing σ and ε with $\Delta\sigma_{loc}/2$ and $\Delta\varepsilon_{loc}/2$, the local deformation range may be expressed as:

$$\frac{\Delta\varepsilon_{loc}}{2} = \left(\frac{\Delta\sigma_{loc}}{2E'}\right) + \left(\frac{\Delta\sigma_{loc}}{2K'}\right)^{1/n'}$$

The Neuber rule relates these local stresses and deformation with the global ones, enabling simple empirically based LCF calculation. To achieve that, two different stress concentration factors are to be defined: K_σ and K_ε, being stress concentration factor and strain concentration factor, respectively:

$$K_\sigma = \frac{\text{maximum local stress}}{\text{global stress}}$$

$$K_\varepsilon = \frac{\text{maximum local strain}}{\text{global strain}}$$

Neuber showed that product of the two concentration factors is constant i.e. that $K_\sigma \cdot K_\varepsilon = K_T^2 = const.$

By defining $K_\sigma = \sigma_{loc}/\sigma$ and $K_\varepsilon = \varepsilon_{loc}/\varepsilon$, where σ and ε are global stress and strain respectively, according to the Neuber rule, it follows:

$$K_\sigma \cdot K_\varepsilon = \frac{\sigma_{loc} \cdot \varepsilon_{loc}}{\sigma \cdot \varepsilon} = K_T^2$$

In the elastic region $\varepsilon = \sigma/E$ and introducing this into equation above:

$$\sigma_{loc} \cdot \varepsilon_{loc} = \frac{\left(K_T^2 \cdot \sigma^2\right)}{E}, \text{ and}$$

$$\Delta\sigma_{loc} \cdot \Delta\varepsilon_{loc} = \frac{\left(K_T^2 \cdot \Delta\sigma^2\right)}{E}$$

Simultaneously solving equations above by iteration it becomes possible to determine the range of local deformations in a function of a given global stress range (Sleczka, 2004).

5.2 *Cumulative HCF and LCF damage*

Hansen and Thayambali, (1995) presented fatigue damage estimation due to a combination of wave load induced HCF and whipping and slamming induced LCF. ISSC, (2000) listed a number of papers analyzing "storm model" assumption—that a ship periodically experience extra high

stresses during sailing in storms. A sequence of storms in time is supposed to affect the damage accumulation.

Urm et al. (2004) made a systematic research of HCF and LCF in ship structural details due to wave loads, within DNV research department, and estimated cumulative fatigue life to be:

$$D = D_{HCF}\left(1 - \frac{\nu_{LCF}}{\nu_0}\right) + \nu_{LCF}\left\{\left(\frac{D_{LCF}}{\nu_{LCF}}\right)^{1/m} + \left(\frac{D_{HCF}}{\nu_0}\right)^{1/m}\right\}^m$$

where:

D_{LCF} = low cycle fatigue damage

$$D_{LCF} = \sum_{i=1}^{k} \frac{n_i}{N_i}$$

D_{HCF} = high cycle fatigue damage

$$D_{HCF} = \frac{\nu_0 T_d}{\bar{a}} \sum_{n=1}^{N_{load}} p_n q_n^m \Gamma\left(1 + \frac{m}{h_n}\right)$$

ν_{LCF} = mean zero-crossing frequency for LCF

ν_0 = mean zero-crossing frequency for HCF.

5.3 *Numerical example*

Numerical example illustrates HCF, LCF and combined HCF and LCF calculation procedure for structural detail on 6500 cbm oceangoing LPG vessel. Cargo is transported in one 4500 m^3 bilobe tank and one 2000 m^3 cylindrical tank. Detailed description of the ship and cargo tanks is given in Rudan and Senjanović, (2005). Hydrodynamic, finite element and stochastic calculations are performed using SESAM software package (DNV, 1998).

Critical structural detail is the Y-joint of shells and longitudinal bulkhead in the bilobe tank. Due to difficulties in manufacturing process a misalignment of shells occur during welding and an eccentricity is introduced into what should be a perfect Y-joint, Figure 24. Tanks are designed and behave as membrane structures and can stand the bending stress due to Y-joint misalignment only to a certain extent.

Eleven Y-joint models are generated employing the volume finite elements with eccentricity ranging from $e = 0$ mm to $e = 20$ mm in step of 2 mm. The model with $e = 14$ mm is presented in Figure 24. Y-joint welds are modelled and the exact hot-spot and notch stresses are determined using linear stress extrapolation, from two neighbouring finite elements, to the weld toe.

Resulting von Misses stress for different values of eccentricities is presented in Table 6. The details of calculation procedure are given by Rudan and Senjanović, (2005). Note that the yield stress for tank material is 390 N/mm^2 and tensile strength is 540 N/mm^2. Therefore, even minor eccentricities leads to unacceptable high stress values and eccentricities exceeding 10 mm may be considered critical and need to be controlled.

5.3.1 *Spectral fatigue analysis*

Spectral HCF analysis is performed for the LPG vessel in concern, for various amounts of joint imperfection (eccentricity from 0 to 20 mm). Hydrodynamic analysis based on strip theory is performed. A ship is divided into 56 strips, Figure 33, and subjected to a number of analyses: two loading conditions (full and ballast), 30 different wave lengths (ranging from 0.105 to 2.6 ship lengths), 13 different heading angles (from 0 to 180 degrees in increments of 15 degrees) and for one ship speed. Thus, in addition to hydrostatic analysis, a total of 780 different load cases are analyzed in both real and imaginary domain for each loading condition.

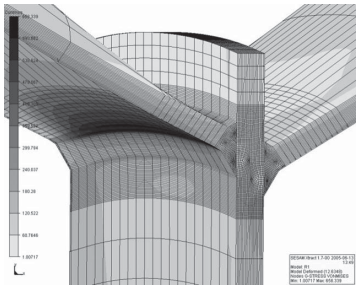

Figure 24. Solid element FE model of Y-joint, eccentricity e = 14 mm.

Table 6. Notch stress concentration factors as a function of Y-joint eccentricity.

	Eccentricity	σ_{vMt}
Model 0	0 mm	213
Model 1	2 mm	338
Model 2	4 mm	384
Model 3	6 mm	431
Model 4	8 mm	510
Model 5	10 mm	567
Model 6	12 mm	584
Model 7	14 mm	679
Model 8	16 mm	715
Model 9	18 mm	819
Model 10	20 mm	845

Calculated hydrodynamic loads are then transferred to FE model, Figure 25 and structural analysis is performed. Transfer of loads is performed automatically by SESAM software package. Coarse mesh finite element model of the entire LPG ship, including cylindrical and bilobe tanks, is generated. A super element modelling technique is used. Direct mesh refinement is applied in the critical Y-joint area.

The entire model consists of some 170,000 shell finite elements and some 140,000 nodes. The model is subjected to each of 780 load cases which consist of: wave pressure at the wet hull surface, inertial forces and internal tank pressure. As a result of structural analysis a set of notch stress transfer functions for Y-joint are obtained, Figure 27.

The stochastic analysis is performed for both loading conditions, the entire range of the Y-joint eccentricities and for the North Atlantic sea-state condition. As a result long-term stress distribution is obtained. Table 7 presents the Weibull distribution parameters for different values of the Y-joint eccentricity.

Fatigue damage results are presented in Table 3. The analysis revealed that full loading condition is the main cause of fatigue damage. It is also clear from Table 8 that eccentricity of 12 mm ($D_{HCF} < 1$) may be tolerated when considering high cycle fatigue damage analysis only, assuming a life time of ship in service of 25 years.

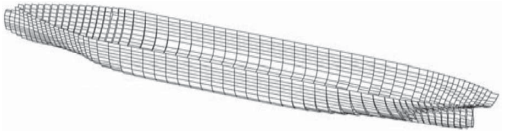

Figure 25. Strip model of LPG ship.

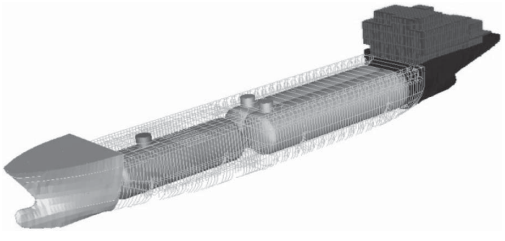

Figure 26. Finite element model of LPG—part of hull hidden.

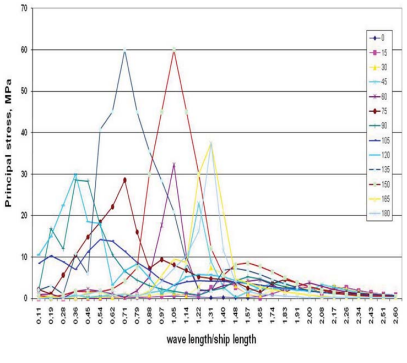

Figure 27. Notch stress transfer functions for Y-joint detail, full loading-real component.

5.3.2 *Low cycle fatigue analysis*

LPG ships in service operate worldwide, usually on a fixed sailing route under a long-term contract. The tank is loaded at the terminal of departure and then emptied at the terminal of arrival. The pressure in the tank oscillates between approximately 0 bars and design pressure of 5 bars in the case of a bilobe tank on LPG carrier. Assuming that no damage occurs during voyage (between terminals),

Table 7. Weibull parameters for ballast (LCO3) and full (LC05) loading condition.

$K_{scf,e}/K_{scf,0}$	LC03			LC05		
	q	h	T0	q	h	T0
1.000	3.354	0.789	8.667	8.473	0.798	8.744
1.271	4.263	0.789	8.667	10.770	0.798	8.744
1.442	4.837	0.789	8.667	12.220	0.798	8.744
1.618	5.423	0.789	8.667	13.700	0.798	8.744
1.948	6.531	0.789	8.667	16.500	0.798	8.744
2.131	7.149	0.789	8.667	18.060	0.798	8.744
2.191	7.351	0.789	8.667	18.570	0.798	8.744
2.562	8.594	0.789	8.667	21.710	0.798	8.744
2.697	9.045	0.789	8.667	22.850	0.798	8.744
3.108	10.427	0.789	8.667	26.340	0.798	8.744
3.207	10.759	0.789	8.667	27.180	0.798	8.744

Table 8. HCF fatigue damage as a function of Y-joint eccentricity.

e, mm	LC03	LC05	D_{HCF}	Fatigue life, years
0	0.005	0.064	0.069	362.617
2	0.010	0.132	0.142	176.587
4	0.014	0.192	0.207	120.878
6	0.020	0.271	0.291	85.792
8	0.035	0.474	0.509	49.108
10	0.046	0.621	0.668	37.446
12	0.050	0.675	0.726	34.449
14	0.081	1.079	1.160	21.559
16	0.094	1.258	1.352	18.489
18	0.144	1.927	2.071	12.071
20	0.158	2.117	2.276	10.986

Table 9. Estimated LCF life-time of Y-joint.

e, mm	Hot spot principal stress [N/mm^2]	Notch stress conc. Factor	Notch strain range [mm]	DLCF	Estimated life [years]
0	307	2,51	0.00231	0,492	50,8
2	389,5	3,19	0.00512	2,101	11,9
4	442	3,62	0.00633	3,472	7,2
6	496	4,06	0.00772	5,434	4,6
8	597,5	4,89	0.01025	10,869	2,3
10	654	5,35	0.01229	14,705	1,7
12	672,5	5,50	0.01291	16,667	1,5
14	786	6,43	0.01669	27,778	0,9
16	828	6,77	0.01818	35,714	0,7
18	953	7,80	0.02285	50,000	0,5
20	984,5	8,05	0.02412	62,500	0,4

oscillation of the global stresses in the tank will follow a stable pattern (Røren et al. 1975).

Roots of the notches and any other highly stressed local areas will inevitably be subjected to the low cycle fatigue damage. LCF life may be calculated according to the Morrow equation, including the correction for the mean stress effects (Xu, 1997), that relates fatigue life, N_f to the maximum local strain amplitude, $\Delta\varepsilon_{loc}$:

$$\frac{\Delta\varepsilon_{loc}}{2} = \frac{\left(\sigma_f' - \sigma_{mean}\right)}{E}\left(2N_f\right)^b + \varepsilon_f'\left(2N_f\right)^c$$

where σ_f' is fatigue strength coefficient, σ_{mean} is the mean stress, b is fatigue strength exponent, ε_f' is fatigue ductility coefficient, c is fatigue ductility exponent and E is the Young's modulus of elasticity. The fatigue properties of SAE1020 are used for LCF calculation: $E = 2.05$ GPa, $K' = 941$ MPa, $n' = 0.18$, $\sigma_f' = 815$ MPa, $\varepsilon_f' = 0.25$, $b = -0.114$, $c = -0.53$.

Fatigue life is estimated as a parameter of the Y-joint eccentricity e and with the assumption of 5 days load cycle for typical LPG carrier. Nominal stress in the Y-joint is chosen to be $\sigma_N = \sigma_{vMt} = 183.34$ MPa as this is theoretical stress in the Y-joint excluding the effects of weld geometry, notch presence and eccentricity (i.e. $e = 0$ mm). Table 9 lists the results.

The LPG tank material is 5% nickel steel, a high-strength material with excellent cryogenic properties. Assuming fatigue properties of SAE1020 steel all the results will be on the conservative side by the unknown scale. However, results clearly indicate the strong influence of rather small eccentricity (imperfection) to the estimated LCF lifetime of Y-joint.

5.3.3 *Combined HCF and LCF*

Combined HCF+LCF life for Y-joint is calculated according to linear life model, (Urm et al. 2004).

Table 10. Combined HCF and LCF fatigue damage.

e [mm]	HCF [years]	LCF [years]	Total life Linear life model [years]	Total life Urm et al. (2004) [years]
0	362.617	50.8	44.558	0.561
2	176.587	11.9	11.149	2.242
4	120.878	7.2	6.795	3.679
6	85.792	4.6	4.366	5.726
8	49.108	2.3	2.197	11.379
10	37.446	1.7	1.626	15.374
12	34.449	1.5	1.437	17.392
14	21.559	0.9	0.864	28.937
16	18.489	0.7	0.674	37.066
18	12.071	0.5	0.480	52.071
20	10.986	0.4	0.386	64.776

Mean zero-crossing frequency for LCF was calculated on the basis of 25 year-service life of LPG and 5 days load-unload period. Mean zero-crossing frequency for HCF was calculated according to simplified expression in Urm et al. (2004). Full loading condition (LC05) is taken into account. Results are presented in Table 10.

Due to a large influence of LCF, total fatigue life is close to LCF life estimation. Results are considered conservative in relation to LCF analysis. Even so, a decrease of total fatigue life due to combination of HCF and LCF effects is clear.

6 FATIGUE ASSESSMENT OF A VERY FAST FERRY SUBJECTED TO COMBINED LOAD

This chapter aims to provide guidelines on the fatigue assessment of the very fast ferries. These are special type of ships that operate at high service speeds, which impose significant demands on

the hull and structure. Apart from hydrodynamic properties, which will not be considered here, their structural properties are in the function of achieving desired speed: very fast ferries have lightweight structure, aluminium and/or high-tensile strength steels are used as construction materials and specific structural details are used to further reduce weight or handle stress concentration. This makes fatigue assessment of such vessels to stand out of common fatigue analysis procedures and require special approach.

Novel trapezoidal longitudinal beams are considered to be feasible alternative to classic deck stiffeners. However, they alone need to be carefully verified against permissible stress and fatigue. In addition, they are subjected to various types of loading acting simultaneously, each with particular contribution.

A procedure for the analysis of critical hot spots on trapezoid longitudinal will be presented. Then, existing loads, both of high and low occurrence frequency, will be taken into account and structural analysis performed, followed by the fatigue analysis. As a result a comprehensive fatigue assessment procedure for fast ferry ships will be established.

6.1 *Fatigue considerations*

Very fast ferries transport cars and passengers at high service speeds that are possible due to their lightweight hull construction and structural details design. By adopting high strength steels, instead of traditional mild steel, designers are able to obtain structure that can withstand high service loads and at the same time have minimum weight. However, this comes at cost of having highly stressed structure and, in particular, very high stress concentration in critical structural details and joints. Current Rules, for example (DnV, 2008), exclude "high speed light crafts" from fatigue assessment procedures. In addition, the mentioned Classification Note "is valid for steel material with yield stress less than 500 MPa", and therefore it is not applicable to very high strength steels (VHTS) having yield stress up to 690 MPa.

An example of structural elements that need new design are profiles for reducing the unsupported span of the (e.g. car deck) plating, as there are no conventional rolled profiles made of VHTS available. Trapezoid profiles, used in bridges, represent an alternative design but the experience gained from civil engineering cannot be directly applicable to marine structures. It is known from their use in bridge construction that trapezoidal longitudinals are prone to fatigue failure due to very large number of load cycles arising from the ongoing traffic. In the case of ship structures the number of load cycles is lower but the distribution of the loads is much more critical.

Special trapezoid shaped longitudinals are designed to support vehicle deck as stiffeners. The advantage of using longitudinals of such a shape is, among other, their good strength/weight ratio. Such longitudinals are relatively wide and therefore provide satisfactory support for a deck plate, permitting its thickness to be only 4 mm, when stiffeners are adequately close to each other.

Spot-weld and the all-weld connections with the deck plate are possible. Spot-weld connection refers to the welding of the stiffeners using a spot-weld technique while the all-weld connection refers to classical, continuous welding along the longitudinal length. Finite element and fatigue analyses needs to be performed to locate and evaluate stresses in trapezoidal longitudinal for both cases.

6.2 *FEM and fatigue analysis*

The aim of the finite element analysis is to locate, evaluate and compare the stresses in trapezoid longitudinals for all weld and spot weld connection. The finite element analysis has to be performed on two levels: global and detailed local analysis.

The global finite element model of the mid ship part of the very fast ferry is generated and subjected to two different loading conditions, one for the ship in hogging and another for the ship in sagging. In both cases additional design pressure load is applied on the corresponding decks.

Detailed finite element analysis is performed to obtain critical hot spot stresses and overall stress distribution. The trapezoid stiffeners are supported by the transverse frames and subjected axially to vertical hull girder bending moment and by transverse force due to the presence of truck load. The hot spots are analyzed for the combination of axial and transversal loads. As a result of the performed analysis stress concentration factors are defined and subsequently used for fatigue damage.

Due to complexity of the deck geometry and a large number of the welded joints, fatigue cracks may start from several locations. A discussion of possible locations of crack initiation is given by Garbatov et al. (2003). The fatigue study presented here will be concerned only with the mid span welded connection.

Fatigue damage assessment is accomplished by simplified approach in several calculation steps. The considered fatigue loading consists of the wave and slamming induced loads and truck breaking load. Details on the load modelling are reported by Garbatov et al. (2005).

Fatigue damage assessment is based on the hot spot stress approach (Fricke and Petershagen, 1992 and Niemi, 1995). Calculated local stresses

around the highly stressed locations depend very much on the structural idealization, the element types used and the mesh subdivision. The application of the mentioned approach has been reported by Garbatov et al. (2002b) and Rudan et al. (2003). For the application of the fracture mechanics approach an application can be seen for example by Garbatov et al. (2003).

6.3 *FEM analysis—application example*

Strength and fatigue assessment, including the comments on modelling and analysis, will be presented as a guideline on how to perform FEM and fatigue analysis of the very fast ferry or similar type of vessel. Detailed description of the global and local models, analysis procedures and results are presented in Garbatov et al. (2010).

6.3.1 *Global finite element model*

Entire ship model or three-hold model is normally used for the global deformation analysis of the large merchant ships. Since fast-ferry ships differ largely from merchant ships, the mentioned method cannot be applied directly.

The global FE ferry model shall contain all the elements that contribute to the longitudinal strength. In the present analysis three types of beam elements are used: trapezoidal longitudinals, HP longitudinals and shell longitudinals. The length of the global model in longitudinal direction, i.e. x-axis, is 36 meters. With the ship breadth of 24.70 m this is being considered to be sufficient in size for global deformation analysis, Figure 28.

The fast ferry is carrying cars and trucks parked on several decks. During the voyage the deck plate and the attached stiffeners are subjected, in general, to four types of loading.

First, a global load due to still water and wave induced bending moments. These loads may be modelled as axial forces applied to the deck structure.

Second, a local load generated from the weight of transported vehicles and transmitted to the stiffened deck plate via vehicle tires.

Third, loads arising from the slamming response. They are characterized by a short loading period, which in combination with the relatively high speed of the ship results in a severe hydrodynamic impact. Slamming causes a sudden vertical acceleration and deflection of the bow and excites transient flexural vibration of the hull girder i.e. whipping. (Senjanović et al. 2003).

Fourth, the load arising from the car breaking during parking.

To properly take into account both global and local loads, two-step sub model finite element analysis is performed based on Det Norske Veritas SESAM package. The global model consists of

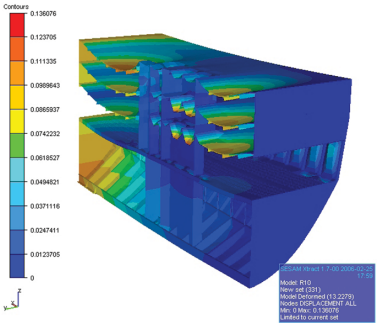

Figure 28. Global model deformation, sagging.

10,034 2-node beam elements, 9,802 4-node shell elements and 6,626 3-node shell elements. It has a total of 74,640 degrees of freedom. The vibratory hull girder bending stress (whipping stress) and breaking load are of much higher frequency than the wave induced stress, and are effectively superimposed (Garbatov et al. 2005).

Boundary conditions are defined in a way that the aft side cross-section is fixed in all degrees of freedom, while the fore side cross-section is rigid, so that sections may remain in plane after the load is applied (sectional moments). In this way symmetry of the load and boundary conditions is satisfied.

The loading applied to the global model consists of sectional design moments, transverse pressure loads on decks and water induced pressure load on the hull up to T = 5.5 m, for both hogging and sagging loading condition, Figure 38. All loads are static. Figure 7 summaries the loading applied on the global model. Global model deformations is presented in Figure 28.

6.3.2 *Local finite element model*

Trapezoid longitudinal is made of two parts, being connected at the middle of the span via supporting plate (backing strip). The thickness of both the trapezoid longitudinal and the supporting plate is 4 mm. Trapezoid longitudinal is connected to the deck plate by spot welds. Spot welds along the trapezoidal longitudinal are 20 mm wide and distanced 80 mm from each other. Alternatively, continuous welding is investigated and in that case the longitudinal is continuously welded to the deck plate.

Two local models, spot-weld and all-weld model, are generated using volume finite elements (20-node solid and 15-node solid), so that the weld geometry may be taken properly into account.

Near the supporting plate, i.e. at the middle of the longitudinal span, the neighbouring finite element width varies from 4 mm to 7.5 mm wide. In this way, it does not conform strictly with the usual "txtxt" requirement of the hotspot stress

evaluation procedure, where t is the thickness of the plating. Finite element width variation occurred during precise modelling of supporting plate and surrounding welds and geometry. All-weld model has the same finite element mesh as the spot-weld model, except the weld geometry, so that comparison of the results may be performed. Further details concerning sub-model generation are reported by Garbatov et al. (2002a) and Guedes Soares et al. (2003).

The loading of the local model consists of prescribed displacements from the global model, both in hogging and sagging loading conditions, and a concentrated force due to the breaking load and acting at the middle of the local model span. It is considered that breaking load is acting only during the boarding. Table 12 summarizes the local loading cases.

6.3.3 *Spot-weld finite element analysis*

Spot-weld model stress distribution is shown in Figures 29 and 31, where three types of highly stressed areas may be distinguished (hot spots 1, 2 and 3).

The hot spot 1 is located at the middle of the trapezoid longitudinal span, where the support plate connects two machine-produced longitudinals. The hot spot 1 occurs due to local change in model geometry and stiffness.

The hot spot 2 is located at the middle of the trapezoid longitudinal span, where the support plate is welded to the longitudinal and where both are bent. In certain cases this is the mostly stressed location as it is located both at the middle of the span and it is most distant from the deck plate.

The hot spots 3 are located at the spot-weld locations. There are a series of such hot spots and their presence has been expected since only weld spots are connecting the trapezoid longitudinal and deck plate.

Table 11. Loading of global model.

Structure	Loading	
Deck 5 plates	Cargo Static Load	$P = 3.7$ kN/m^2
Deck 4 plates		$P = 4.1$ kN/m^2
Deck 3 plates		$P = 4.2$ kN/m^2
Deck 2 plates		$P = 15.1$ kN/m^2
Side shell plates	Hydrostatic Pressure	$T = 5.5$ m
NA of Fr 183	Vertical Bending Moment—Hogging	$M_h = 1387$ MNm
NA of Fr 183	Vertical Bending Moment—Sagging	$M_s = -1740$ MNm

Table 12. Local model load cases.

Loading case	Global loading	Local loading
LC1	Bending-Hogging	Without
LC2	Bending-Hogging	Truck load
LC3	Bending-Sagging	Without
LC4	Bending-Sagging	Truck load

6.3.4 *All-weld model stresses*

Three areas of high stress concentration (hot spots 4, 5 and 6) may be observed for the all-weld finite element model, Figure 32. The hot spot 4 on the all-weld model corresponds to the hotspot 2 of the spot-weld model.

The hot spot 5 is shown in Figure 32. The high stress concentration is located at the edge of the small side weld that connects the supporting plate with the trapezoid longitudinal. A view from the "inside" of the trapezoid longitudinal, presenting the hot spot 5 stress concentration is given in Figure 31.

The hot spot 6 in the all-weld model corresponds to the hotspot 3 in the spot-weld model and it is presented with red arrow in Figure 32. Concentrated

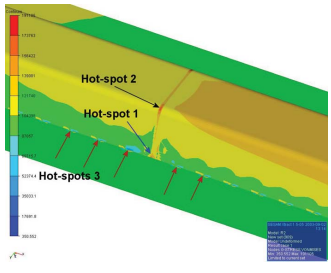

Figure 29. Hot spot 1 to 6 for spot-weld model.

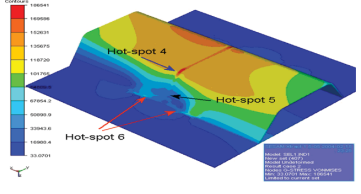

Figure 30. Hot spot 1 to 6 for all-weld model.

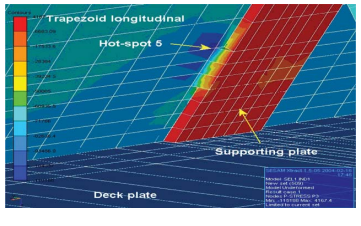

Figure 31. Hot spots 5, all-weld model.

forces are causing the stress concentration in that area. High stress is affecting both the deck plate and the trapezoid longitudinal, so the weld toe becomes a subject for the hot spot stress evaluation. Figure 32 presents the hot spot 6 in detail.

6.3.5 *Hotspot stress analysis*

The aim of the hot spot stress analysis is to evaluate the stress concentration factors for the selected hot spots. The Classification Societies define the hot spot assessment procedure within their fatigue assessment rules. However, no extrapolation procedure covers all possible structural details geometry and/or loads and stress combination. Therefore, careful analysis of the stresses and reasonable stress extrapolation technique should be used.

The stress concentration factor, SCF is commonly defined as the ratio of the hot-spot stress, $\sigma_{hot\text{-}spot}$, and the nominal stress, σ_{nom}, i.e.:

$$SCF = \frac{\sigma_{hot-spot}}{\sigma_{nom}}$$

The hot spot principal stresses are determined by direct computation using finite element analysis. The mesh refinement of the local finite element model is sufficient and with element lengths near high stress zones equal to the plate thickness. A linear extrapolation is employed in hot spot stress calculations. As 20-node solid finite elements are used, nodal stresses were available directly from the solver results. The direction of the principal stresses was examined with the aim of stress vector presentation.

The evaluation of the nominal stresses is not a straightforward task when both complex geometry and stress field are present. In the present analysis a neighbouring "low-gradient" stress is assumed to be a nominal stress. In most cases longitudinal stress coincides with the principal stress and therefore nominal stress, far enough from the highly stresses areas, may be considered as evaluated precisely.

Resulting stress concentration factors are in the range from 1.32 to 2.08 depending on the hot spot location and load case considered.

6.4 *Load considerations*

The trapezoid longitudinal of concern is located below the car deck and it is subjected to both lateral and axial load. The lateral load is provoked by the truck breaking load induced due to the breaking of the truck on the position of parking on the deck. The force applied may be calculated as P = k w, where k is the beam stiffness and w is the beam's displacement.

Bottom slamming is a particularly complex phenomenon. The magnitude and duration of the impact pressure depend strongly on and are sensitive to the angle and the relative shape of the ship

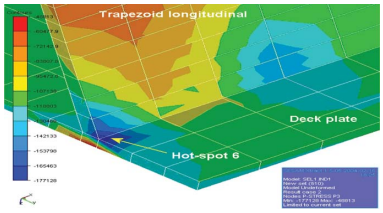

Figure 32. Hot spots 6, all-weld model.

bottom and the water surface, as well as on their relative speed of approach. The slamming has been the subject of significant research effort (Ochi, 1964, Mansour and d' Oliveira, 1975, Ochi and Motter, 1973, Kawakami et al. 1977 and Evans, 1982). To evaluate the slamming effect the relative motion between ship and wave is to be evaluated in the frequency domain or in a more realistic way in the time domain. The relative ship motion permits the estimation of the instant when the impact may occur and its location along the ship, as well as the intensity of the slamming force. Different models are compared by Ramos and Guedes Soares, (1995). The slamming stresses induced to the stiffener are considered as a transient process:

$$\sigma_i(t) = \sigma_{ai} \exp[-k_i \omega_i t] \sin(\omega_i t + \varepsilon_i)$$

where i = 2, 3, σ_{a2} is the excitation nominal stress amplitude, k = 0.08 is a damping factor and ε_2 is the phase angle. The excitation amplitude, σ_{a2}, of the transient process, $\sigma_2(t)$, is considered as a random variable that follows a Rayleigh distribution which implies that the process can be treated as a narrow-banded Gaussian process with time-dependent variance. The combination of $\sigma_1(t)$ and $\sigma_2(t)$ then becomes the sum of a stationary Gaussian process and a transient one. The process differs, but is similar to that of the combination of two stationary processes. Both car breaking and slamming loading induce stresses that result in additional damage to wave induced load damage and they are modelled as transient process. For simplification here, the phase angles are not taken into account.

Wave induced stresses in the welded joints may be described as a Gaussian process with zero mean value. In that case the stress amplitude distribution follows the Rayleigh distribution for any short sea state. The long-term stress distribution is defined on the basis of Rayleigh short sea-state stress distributions. The wave-induced stresses are described as:

$$\sigma_1(t) = \sigma_{a1} \cos(\omega_1 t + \varepsilon_1)$$

where σ_{a1} is the nominal stress amplitude, ω_1 is the natural frequency for the first elastic mode of vibration and ε_1 is phase angle.

Ship motion analysis is performed assuming rigid ship motion. The combination of wave induced load with the loads due to slamming and cargo operation (low and high frequency loads) needs to be taken into account. It was observed that the duration of the impulse force in the case of the bottom slamming is rather small (Lewis and Hoffman, 1973) and is therefore considered as a linear elasto-dynamic problem, which means that the damping coefficient is proportional to the velocity of displacement and the recovering to the initial state force is a linear function.

The excitation amplitude of nominal stresses at the point of study is as a function of the axial load subjected to the structures due to the vertical induced bending moment: $M_a^h = M_W^{Hogging} + M_{Slam}$, and $M_a^s = M_W^{Sagging} + M_{Slam}$ where M_W is the vertical wave induced bending moment for hogging and sagging and M_{Slamm} is the vertical bending moment due to slamming and transfer load due to the car operation on deck. The slamming loads were determined applying only to the sagging condition (Garbatov et al. 2005). The ship length, the mass distribution, the sectional breadths and the ship speed serve as input. Furthermore, the vertical acceleration versus the ship length is needed for the determination of the maximum hydrodynamic pressure and the inertia forces.

6.5 *Fatigue assessment*

The stress range, $\Delta\sigma_i$, may be calculated as:

$$\Delta\sigma_{i,n} = \left(\sigma_{i,a,tensile} - \sigma_{i,a,compressive}\right)$$

$$\Delta\sigma_i = SCF\Delta\sigma_{i,n}$$

where SCF is the stress concentration factor of the hotspot considered. For the loads and very fast ferry considered results are as presented in Table 13.

The fatigue damage assessment is based on the Miner, (1945) summation. The basic assumption of the method is that structural damage per load cycle is constant at a given stress range. It is assumed that the stress range is distributed according to a two-parameter Weibull distribution and fatigue damage is calculated as (Nolte and Hansford, 1976):

$$D_{j1} = \frac{\upsilon_o T_d}{K}\frac{\Delta\sigma_{j1}}{\left[Ln(n_o)\right]^{m/a}}\Gamma\left(1+\frac{m}{\alpha}\right)$$

and the fatigue damage for the transient process is calculated (Jiao and Moan, 1990) as:

$$D_{ji} = \frac{\left(2\sqrt{2}\right)^m \Gamma\left(1+\frac{m}{2}\right)\Delta\sigma_{ji}^m}{2K\left[Ln(n_i)\right]^{m/2}\left[1-Exp(-2\pi k_i m)\right]}, i = 2,3$$

where the material descriptors of the S-N curve are taken from Det norske Veritas, (1998) as K = 1012.38, m = 3 and $\upsilon_o = 0.11$, $\alpha = 1$. The number of slamming and car breaking cases during a 20 year service life is considered as an example here as 1622, i = 2 for slamming and i = 3 for car breaking induced load respectively. For any hotspot j fatigue damage is calculated as:

$$D_j = \sum_{i=1}^{3} D_{ji}$$

The overall average fatigue damage of welded joint due to the contribution of different loading is shown in Figures 33 and 51 show the total fatigue damage at any hot spot due to the entered loads. It can be seen from Figures 33 and 51 that in general, fatigue damage is lower for the all-weld model then the spot-weld model. The location of highest fatigue damage for the all-weld longitudinal and

Table 13. Stress range for various hot spots and loadings.

Hotspot, j	$\Delta\sigma_{j2}$, MPa	$\Delta\sigma_{j3}$, MPa	$\Delta\sigma_{j1}$, MPa
1	40.99	77.26	66.61
2	38.73	313.34	66.75
3	40.99	77.26	67.12
4	38.73	313.34	67.68
5	41.51	23.54	68.35
6	40.99	77.26	69.09

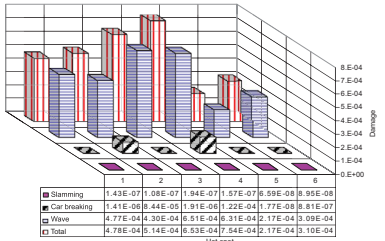

Figure 33. Fatigue damage of Hotspots 1 to 6.

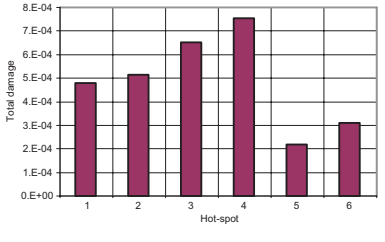

Figure 34. Total fatigue damage of Hotspots 1 to 6.

for the spot-weld longitudinal is the bending of the trapezoid (hotspot 4).

7 CONCLUSION

This paper presented recently developed models for fatigue damage of marine structures accounting for several structural imperfections and different types of loadings. Besides commonly present uncertainties in fatigue ship structural analysis associated with structural modelling and the random wave induced loading various uncertainties arising from imperfection of structural joint that may occur during manufacturing and service life and the interaction between wave induced load and structure have been analyzed. This work also deals with the fatigue assessment of marine structures, describing several steps of the calculation accounting for the combination of low and high-frequency induced loading. Fatigue damage is calculated based on the Palgrem-Miner approach.

ACKNOWLEDGEMENTS

The second author has been funded by a research project "Fatigue Based Design Rules for the Application of High Tensile Steels in Ships, FatHTS", which was partially financed by the European Union through the contract No. CT96-0195 during his visit to the Centre for Marine Technology and Engineering (CENTEC), Technical University of Lisbon.

The third author has been funded by the Portuguese Foundation for Science and Technology (Fundação para a Ciência e a Tecnologia—FCT) under contract SFRH-BD-39106-2007.

More recent results have been obtained within the project "MARSTRUCT—Network of Excellence on Marine Structures" (http://www.mar.ist.utl.pt/marstruct/) and has been partially funded by the European Union through the Growth programme under contract TNE3-CT-2003-506141.

REFERENCES

ANSYS, 2009, Online Manuals, Release 11.

Chakarov, K., Garbatov, Y. and Guedes Soares, C., 2008, Fatigue analysis of ship deck structure accounting for imperfections, *International Journal of Fatigue*, Vol. 30, (10–11), pp. 1881–1897.

Chakarov, K., Garbatov, Y. and Guedes Soares, C., 2007, Hot-Spot Stress Analysis of Deck Structures Subjected to Corrosion and Fatigue, Maritime Industry, *Ocean Engineering and Coastal Resources*, C. Guedes Soares and P. Kolev (Eds), Francis and Taylor, pp. 153–160.

Det norske Veritas, 1998, *SESAM-User Manual*, Hovik, Norway.

Det Norske Veritas, 2008, Fatigue assessment of ship structures.

Dong, P., 2001, A Practical Stress Definition and Numerical Implementation for Fatigue Analyses, *International Journal of Fatigue*, Vol. 23, (10), pp. 865–876.

Evans, J., 1982, Preliminary Design Estimation of Hull Girder Response to Slamming, *Transaction SNAME*, Vol. 90, pp. 55–83.

Fricke, W. and Petershagen, H., 1992, Detail Design of Welded Ship Structures Based on Hot-Spot Stresses, *Proceedings of the Practical Design of Ships and Mobile Units*, J.B. Caldwell and G. Ward, Elsevier Science Limited, Vol. 2, pp. 1087–1100.

Fricke, W. and Petershagen, H., 1992, Detail Design of Welded Ship Structures Based on Hotspot Stresses, *Proceedings of the Practical Design of Ships and Mobile Units*, Vol. 2, Elsevier Science Limited, pp. 1087–1100.

Garbatov, Y. and Guedes Soares, C., 1998, Fatigue Reliability of Maintained Welded Joints in the Side Shell of Tankers, *Journal of Offshore Mechanics and Arctic Engineering*, Vol. 120, pp. 2–9.

Garbatov, Y., Rudan, S. and Guedes Soares, C., 2002a, Application of the Spectral Approach for Fatigue Analysis of Marine Structural Details, *Proceedings of the XIth International Maritime Association of Mediterranean Congress* (IMAM2002), pp. 1–6.

Garbatov, Y., Rudan, S. and Guedes Soares, C., 2002b, Fatigue Damage of Structural Joints Accounting for Nonlinear Corrosion, *Journal of Ship Research*, Vol. 46, pp. 289–298.

Garbatov, Y., Rudan, S. and Guedes Soares, C., 2003, Fatigue Life Evaluation of Ship Knuckle Detail Based on Fracture Mechanics and Fatigue Test, *Journal of Offshore Mechanics and Arctic Engineering*, Vol. 126, No. 1, pp. 139–145.

Garbatov, Y., Rudan, S. and Guedes Soares, C., 2010, Fatigue assessment of welded trapezoidal joints of a very fast ferry subjected to combined load, *Engineering Structures*, Vol. 32, pp. 800–807.

Garbatov, Y., Santos, J.M. and Guedes Soares, C., 2005, Effect of Truck Induced Load on Welded Structural Joints Subjected to Fatigue, *Maritime Transportation and Exploitation of Ocean and Coastal Resources*, C. Guedes Soares, Y. Garbatov, N. Fonseca (Eds.), Francis and Taylor, Vol. 1, pp. 387–394.

Gaspar, B., Garbatov, Y. and Guedes Soares, C., 2009, Effect of uncertain Weld Shape on the Structural Hot-spot Stress Distribution, *Analysis and Design of Marine Structures*, C. Guedes Soares and P.K. Das (Eds), Francis and Taylor, pp. 267–278.

Guedes Soares, C. and Garbatov, Y., 1998, Reliability of Maintained Ship Hull Subjected to Corrosion and Fatigue, *Structural Safety*, 20, pp. 201–219.

Guedes Soares, C. and Garbatov, Y., 1999, Reliability of Maintained, Corrosion Protected Plates Subjected to Non-Linear Corrosion and Compressive Loads, *Marine Structures*, pp. 425–445.

Guedes Soares, C. and Moan, T., 1991, Model Uncertainty in the Long-term Distribution of Wave-induced Bending Moment for Fatigue Design of Ship Structure, *Marine Structures*, 4, pp. 295–315.

Guedes Soares, C., Garbatov, Y. and von Selle, H., 2003, Fatigue Damage Assessment of Ship Structural Components Based on the Long-term Distribution of Local Stresses, *International Shipbuilding Progress*, Vol. 50, pp. 35–56.

Guedes Soares, C., Garbatov, Y., Zayed, A. and Wang, G., 2005, Non-linear Corrosion Model for Immersed Steel Plates Accounting for Environmental Factors, *Transactions of the Society of Naval Architects and Marine Engineers,* Vol. 113, pp. 306–322.

Hansen, P. and Thayamballi, A., 1995, Fatigue Damage Considering Whipping Arising from Slamming, *Proceedings of OMAE'95*, pp. 155–163.

Heo, J., Kang, J., Kim, Y., Yoo, I., Kim, K. and Urm, H., 2004. A Study on the Design Guidance for Low Cycle Fatigue in Ship Structure, *Proceeding of the 9th PRADS Symposium*, pp. 782–789.

IACS, 2006, No. 47, *Shipbuilding and Repair Quality Standard*. Revised document 3, London (UK): International Association of Classification Societies Ltd.

IMSL, 1997, Fortran subroutines for statistical applications. *Statistical library*, Vol. 2. San Diego (CA): Visual Numerics Inc.

International Institute of Welding, 1995, *Recommendations on Fatigue of Welded Components*, IIW Document, XIII-1539-95.

Kawakami, M., Michimoto, J. and Kobashi, K., 1977, Prediction of Long-term Whipping Vibration Stress to Slamming of Large Full Ship in Rough Seas, *International Shipbuilding Progress*, Vol. 24, pp. 83–110.

Lewis, E.V. and Hoffman, D., 1973, Load Criteria for Ship Structural Design, *Ship Structure Committee*, Vol. 240, Washington, USA.

Mansour, A. and d'Oliveira J., 1975, Hull Bending Moment due to Ship Bottom Slamming in Regular Wave, *Journal of Ship Research*, Vol. 19, No. 2, pp. 80–92.

Melchers, R., 1999, *Structural reliability analysis and prediction*. Sussex (UK), John Wiley & Sons.

Melchers, R., 1998, Probabilistic Modelling of Immersion Marine Corrosion, *Structural Safety and Reliability*, Balkema, pp. 1143–1149.

Melchers, R., 2003, Mathematical Modelling of the Diffusion Controlled Phase in Marine Immersion Corrosion of Mild Steel, *Corrosion Science*, 45, pp. 923–940.

Niemi, E., 1992, Determination of Stresses for Fatigue Analysis of Welded Components, *Proceedings of the IIW, Conference on Design in Welded Construction*, pp. 57–74.

Niemi, E., 1995, Recommendation Concerning Stress Determination for Fatigue Analysis of Weld Components: Abington Publishing.

Niemi, E., Fricke, W. and Maddox, S. 2004, *Structural Stress Approach to Fatigue Analysis of Welded Components*—Designer's Guide. In: IIW Doc. XIII-1819-00/XV-1090-01.

Nolte, K. and Hansford, J., 1976, Closed-form expressions for determining the fatigue damage of structures due to ocean waves, *Proceedings Offshore Technology Conference*, pp. 861–870.

Ochi, M. and Motter, L., 1973, Prediction of Slamming Characteristics and Hull Responses for Ship Design, *Transaction SNAME*, Vol. 24, pp. 83-110.

Ochi, M., 1964, Prediction of Occurrence and Severity of Ship Slamming at Sea, *Proceedings of the 5th Symposium on Naval Hydrodynamics*, Vol. ACR 112, Office of Naval Research.

Paik, J., Lee, J., Hwang, J. and Park, Y., 2003, A Time-Dependent Corrosion Wastage Model for the Structures of Single and Double Hull Tankers and FSOs, *Marine Technology*, Vol. 40, pp. 201–217.

Panayotova, M., Garbatov, Y. and Guedes Soares, C., 2004a, Factor Influencing Corrosion of Steel Structural Elements Immersed in Seawater, *Proceedings of the International Conference on Marine Science and Technology*, pp. 280–286.

Panayotova, M., Garbatov, Y. and Guedes Soares, C., 2004b, Factor Influencing Atmospheric Corrosion and Corrosion in Closed Spaces of Marine Steel Structures, *Proceedings of the International Conference on Marine Science and Technology*, pp. 286-292.

Paris, P. and Erdogan, F., 1963, A Critical Analysis of Crack Propagation Laws, *Journal of Basic Engineering*, ASME, Vol. 85, pp. 528–534.

Petershagen, H., Fricke, W. and Massel, T. 1991, Application of the Local Approach to the Fatigue Strength Assessment of Welded Structures in Ships. In: IIW, XIII-1409-91, 1991.

Radaj, D., 1990, Design and Analysis of Fatigue-Resistant Welded Structures, Cambridge, Abington Publishing.

Ramos, J. and Guedes Soares, C., 1995, Vibratory Response of Ship Hulls to Wave Impact Loads, *International Shipbuilding Progress*, Vol. 45, pp. 71–87.

Røren, E., Vedeler, B., Flatseth J. and Johannessen, T., 1975, *Design of ships carrying LPG and LNG*, Det Norske Veritas.

Rudan, S. and Senjanović, I., 2005, "Fatigue Strength Assessment of a Weld Connection Misalignment in LPG Bilobe Cargo Tanks", *Maritime Transportation and Exploitation of Ocean and Coastal Resources*, C. Guedes Soares, Y. Garbatov, N. Fonseca (Eds.), Francis and Taylor, pp. 512–526.

Rudan, S., Garbatov, Y. and Guedes Soares, C., 2003, Fatigue Damage Assessment of Side Shell Longitudinal Based on Spectral Approach, *Brodogradnja*, Vol. 51, No. 3, pp. 43–51.

Senjanović, I., Tomašević, S. and Parunov, J., 2003, Ship Slamming and Whipping in Rough Sea, *Brodogradnja*, Vol. 51, No. 1, pp. 45–56.

Sleczka, L. 2004, Low cycle fatigue strength assessment of butt and fillet weld connection, *Journal of Constructional Steel Research,* 60, pp. 701–712.

Technical Committee II.1, 2000, Quasi-Static Response, *Proceedings of the 14th International Ship and Offshore Structures Congress*, Vol. 1, pp. 133-195, Eddited by H. Ohtsubo and Y. Sumi.

Urm, H., Yoo, I., Heo, J., Kim, S., and Lotsberg, I., 2004. Low Cycle Fatigue Strength Assessment for Ship Structures, *Proceeding of the 9th PRADS Symposium*, pp. 774–781.

Xiao, Z.-G. and Yamada, K., 2004, A Method of Determining Geometric Stress for Fatigue Strength Evaluation of Steel Welded Joints, *International Journal of Fatigue*, 26, pp. 1277–1285.

Xu, T., 1997, Fatigue of Ship Structural Details—Technical Development and Problems, *Journal of Ship Research*, Vol. 41, pp. 318–331.

Yamamoto, N. and Ikagaki, K., 1998, A Study on the Degradation of Coating and Corrosion on Ship's Hull Based on the Probabilistic Approach, *Journal of Offshore Mechanics and Arctic Engineering*, Vol. 120, pp. 121–128.